Ultra-broadband THz time-domain spectroscopy of common polymers using THz air photonics

D'Angelo, Francesco; Mics, Zoltán; Bonn, Mischa; Turchinovich, Dmitry

Published in:
Optics Express

Link to article, DOI:
10.1364/OE.22.012475

Publication date:
2014

Document Version
Publisher's PDF, also known as Version of record

Ultra-broadband THz time-domain spectroscopy of common polymers using THz air photonics

Francesco D'Angelo,[1] Zoltán Mics,[1] Mischa Bonn,[1] and Dmitry Turchinovich[1,2,*]

[1]*Max Planck Institute for Polymer Research, Ackermannweg 10, Mainz, 55128, Germany*
[2]*DTU Fotonik, Technical University of Denmark, Ørsteds Plads 343, 2800 Lyngby, Denmark*
[*]*turchino@mpip-mainz.mpg.de*

Abstract: Terahertz-range dielectric properties of the common polymers low-density polyethylene (LDPE), cyclic olefin/ethylene copolymer (TOPAS®), polyamide-6 (PA6), and polytetrafluoroethylene (PTFE or Teflon®) are characterized in the ultra-broadband frequency window 2-15 THz, using a THz time-domain spectrometer employing air-photonics for the generation and detection of single-cycle sub-50 fs THz transients. The time domain measurements provide direct access to both the absorption and refractive index spectra. The polymers LDPE and TOPAS® demonstrate negligible absorption and spectrally-flat refractive index across the entire spectroscopy window, revealing the high potential of these polymers for applications in THz photonics such as ultra-broadband polymer-based dielectric mirrors, waveguides, and fibers. Resonant high-frequency polar vibrational modes are observed and assigned in polymers PA6 and PTFE, and their dielectric functions in the complete frequency window 2-15 THz are theoretically reproduced. Our results demonstrate the potential of ultra-broadband air-photonics-based THz time domain spectroscopy as a valuable analytic tool for materials science.

OCIS codes: (300.6495) Spectroscopy, terahertz; (160.5470) Polymers; (320.7150) Ultrafast spectroscopy.

References and links

1. D. H. Auston and M. C. Nuss, "Electrooptic generation and detection of femtosecond electrical transients," IEEE J. Quantum Electron. **24**(2), 184–197 (1988).
2. D. Grischkowsky, S. Keiding, M. Van Exter, and C. Fattinger, "Far-infrared time-domain spectroscopy with terahertz beams of dielectrics and semiconductors," J. Opt. Soc. Am. B **7**(10), 2006–2015 (1990).
3. B. Ferguson and X.-C. Zhang, "Materials for terahertz science and technology," Nat. Mater. **1**(1), 26–33 (2002).
4. P. U. Jepsen, D. G. Cooke, and M. Koch, "Terahertz spectroscopy and imaging - Modern techniques and applications," Laser Photon. Rev. **5**(1), 124–166 (2011).
5. S. Wietzke, C. Jansen, M. Reuter, T. Jung, D. Kraft, S. Chatterjee, B. M. Fischer, and M. Koch, "Terahertz spectroscopy on polymers: A review of morphological studies," J. Mol. Struct. **1006**(1–3), 41–51 (2011).
6. N. Nagai and R. Fukasawa, "Abnormal dispersion of polymer films in the THz frequency region," Chem. Phys. Lett. **388**(4–6), 479–482 (2004).
7. P. D. Cunningham, N. N. Valdes, F. A. Vallejo, L. M. Hayden, B. Polishak, X.-H. Zhou, J. Luo, A. K.-Y. Jen, J. C. Williams, and R. J. Twieg, "Broadband terahertz characterization of the refractive index and absorption of some important polymeric and organic electro-optic materials," J. Appl. Phys. **109**(4), 043505 (2011).
8. B. Scherger, M. Scheller, C. Jansen, M. Koch, and K. Wiesauer, "Terahertz lenses made by compression molding of micropowders," Appl. Opt. **50**(15), 2256–2262 (2011).
9. K. Nielsen, H. K. Rasmussen, A. J. L. Adam, P. C. Planken, O. Bang, and P. U. Jepsen, "Bendable, low-loss Topas fibers for the terahertz frequency range," Opt. Express **17**(10), 8592–8601 (2009).
10. D. Turchinovich, A. Kammoun, P. Knobloch, T. Dobbertin, and M. Koch, "Flexible all-plastic mirrors for the THz range," Appl. Phys., A Mater. Sci. Process. **74**(2), 291–293 (2002).
11. Q. Wu and X.-C. Zhang, "7 terahertz broadband GaP electro-optic sensor," Appl. Phys. Lett. **70**(14), 1784–1786 (1997).
12. Q. Wu, M. Litz, and X. C. Zhang, "Broadband detection capability of ZnTe electro-optic field detectors," Appl. Phys. Lett. **68**(21), 2924–2926 (1996).

#208438 - $15.00 USD Received 17 Mar 2014; revised 9 May 2014; accepted 9 May 2014; published 15 May 2014

13. N. Karpowicz, J. Dai, X. Lu, Y. Chen, M. Yamaguchi, H. Zhao, X.-C. Zhang, L. Zhang, C. Zhang, M. Price-Gallagher, C. Fletcher, O. Mamer, A. Lesimple, and K. Johnson, "Coherent heterodyne time-domain spectrometry covering the entire "terahertz gap"," Appl. Phys. Lett. **92**(1), 011131 (2008).
14. N. Karpowicz, X. Lu, and X.-C. Zhang, "Terahertz gas photonics," J. Mod. Opt. **56**(10), 1137–1150 (2009).
15. J. Liu and X. C. Zhang, "Birefringence and absorption coefficients of alpha barium borate in terahertz range," J. Appl. Phys. **106**(2), 023107 (2009).
16. M. Zalkovskij, C. Zoffmann Bisgaard, A. Novitsky, R. Malureanu, D. Savastru, A. Popescu, P. Uhd Jepsen, and A. V. Lavrinenko, "Ultrabroadband terahertz spectroscopy of chalcogenide glasses," Appl. Phys. Lett. **100**(3), 031901 (2012).
17. N. Vieweg, B. M. Fischer, M. Reuter, P. Kula, R. Dabrowski, M. A. Celik, G. Frenking, M. Koch, and P. U. Jepsen, "Ultrabroadband terahertz spectroscopy of a liquid crystal," Opt. Express **20**(27), 28249–28256 (2012).
18. D. J. Cook and R. M. Hochstrasser, "Intense terahertz pulses by four-wave rectification in air," Opt. Lett. **25**(16), 1210–1212 (2000).
19. K. Y. Kim, A. J. Taylor, J. H. Glownia, and G. Rodriguez, "Coherent control of terahertz supercontinuum generation in ultrafast laser–gas interactions," Nat. Photonics **2**(10), 605–609 (2008).
20. N. Karpowicz and X.-C. Zhang, "Coherent terahertz echo of tunnel ionization in gases," Phys. Rev. Lett. **102**(9), 093001 (2009).
21. A. Nahata and T. F. Heinz, "Detection of freely propagating terahertz radiation by use of optical second-harmonic generation," Opt. Lett. **23**(1), 67–69 (1998).
22. Y. S. You, T. I. Oh, and K. Y. Kim, "Off-axis phase-matched terahertz emission from two-color laser-induced plasma filaments," Phys. Rev. Lett. **109**(18), 183902 (2012).
23. P. Klarskov, A. C. Strikwerda, K. Iwaszczuk, and P. U. Jepsen, "Experimental three-dimensional beam profiling and modeling of a terahertz beam generated from a two-color air plasma," New J. Phys. **15**(7), 075012 (2013).
24. I. Pupeza, R. Wilk, and M. Koch, "Highly accurate optical material parameter determination with THz time-domain spectroscopy," Opt. Express **15**(7), 4335–4350 (2007).
25. P. U. Jepsen and B. M. Fischer, "Dynamic range in terahertz time-domain transmission and reflection spectroscopy," Opt. Lett. **30**(1), 29–31 (2005).
26. S. Krimm, C. Y. Liang, and G. B. B. M. Sutherland, "Infrared spectra of high polymers. II. Polyethylene," J. Chem. Phys. **25**(3), 549–562 (1956).
27. J. R. Birch, "The far infrared optical constants of polyethylene," Infrared Phys. **30**(2), 195–197 (1990).
28. G. W. Chantry, J. W. Fleming, E. A. Nicol, H. A. Willis, M. E. A. Cudby, and F. J. Boerio, "The far infra-red spectrum of crystalline polytetrafluoroethylene," Polymer **15**(2), 69–73 (1974).
29. G. W. Chantry, E. A. Nicol, R. G. Jones, H. A. Willis, and M. E. A. Cudby, "On the vibrational assignment problem for polytetrafluoroethylene: 1. The far infra-red spectrum," Polymer **18**(1), 37–41 (1977).
30. P. Dannetun, M. Schott, and M. Rei Vilar, "High-resolution electron energy loss spectroscopy of thin crystalline highly oriented films of poly(tetrafluoroethylene)," Thin Solid Films **286**(1–2), 321–329 (1996).
31. C. Y. Liang and S. Krimm, "Infrared spectra of high polymers. III. Polytetrafluoroethylene and Polychlorotrifluoroethylene," J. Chem. Phys. **25**(3), 563–571 (1956).
32. V. A. Bershtein and V. A. Ryzhov, "Relationship between molecular characteristics of polymers and parameters of far-infrared spectra," J. Macromol. Sci. Part B Phys. **23**(2), 271–287 (1984).
33. W. F. X. Frank and H. Fiedler, "On the problem of direct observation of H-bridge interactions in polymers by FIR spectroscopy," Infrared Phys. **19**(3–4), 481–489 (1979).
34. I. Matsubarai and J. H. Magill, "Lower-frequency infrared spectra and structures of some typical aliphatic polyamides*," J. Polym. Sci., Polym. Phys. Ed. **11**, 1173–1187 (1973).
35. H. Tadokoro, "Structural studies of polyesters. II. Far-infrared spectra of aliphatic polyesters: comparison with α-polyamides," J. Chem. Phys. **49**(8), 3359–3373 (1968).
36. E. S. Clark, "The molecular conformations of polytetrafluoroethylene: forms II and IV," Polymer **40**(16), 4659–4665 (1999).
37. M. Dressel and G. Grüner, *Electrodynamics of Solids* (Cambridge University, 2002).

1. Introduction

THz time-domain spectroscopy (THz TDS) is a commonly used, phase-sensitive method to measure the complex-valued dielectric function of materials in the THz spectral window. This technique is traditionally based on the nonlinear-optical or photo-conductive conversion of femtosecond laser pulses into single-cycle THz transients. The detection of these THz waveforms is again enabled by ultra-short laser pulses, using either electro-optic or photoconductive sampling [1–4]. In this way the effect on the THz pulse propagating through the material of interest can be measured directly in time domain. Due to their ultra-short duration, the THz waveforms used for THz TDS contain a broad frequency spectrum. Analysis of the measured time domain THz signals in the frequency domain provides the THz frequency-resolved real and imaginary components of the complex-valued dielectric function (or, equivalently, the absorption and refractive index spectra) of the materials of interest.

#208438 - $15.00 USD Received 17 Mar 2014; revised 9 May 2014; accepted 9 May 2014; published 15 May 2014

In polymer science THz TDS is especially useful since it allows access to the spectral region where many interesting collective vibrational modes in macromolecules occur [5–7]. In return, many polymers have found practical applications in THz-range photonics: they are used for THz windows, lenses, waveguides, dielectric mirrors, photonic crystals, etc [8–10]. The accessible spectral window of a traditional THz TDS system, such as based on the nonlinear crystals or photoconductive antennas, is usually limited to 2-4 THz. Most of the bandwidth of the ultra-short laser pulses, used for the THz generation, is not converted into the THz signal due to the material-imposed limitations of the THz emitters and detectors. For nonlinear crystal-based systems, for example, these limitations are due to the THz-range refractive index dispersion and absorption associated with phonon modes of the nonlinear crystals used in the THz spectrometer [11,12].

With the recent advent of THz air-photonics [13,14] the crystal-based limitations of THz TDS can be avoided, providing the opportunity for efficient conversion of the *full* bandwidth of the ultra-short laser pulse into the THz signal. This allows for THz TDS in a significantly extended frequency range, up to 20 THz and beyond, providing indispensable direct information about the properties of the materials in this new frequency range. At the same time, as the THz photonics extends to increasingly higher frequencies, the technologically-relevant materials for ultra-broadband THz photonics components, such as low-loss and non-dispersive dielectrics, must be identified. In this paper we demonstrate the application of the ultra-broadband air-photonics-based THz TDS in both technologically and fundamentally oriented polymer research. Despite the increasing availability of tabletop air-photonics-based THz TDS systems with an exceptionally broad spectral bandwidth, we note that only a very limited number of reports is available in the literature describing the response of different materials in this extended frequency window [15–17].

2. Experimental results and discussion

2.1 Setup and experimental procedure

The schematic of our ultra-broadband THz setup is illustrated in Fig. 1. A Ti:sapphire amplified laser system (Spitfire ACE by Spectra-Physics) producing ultra-short laser pulses of ~40 fs duration at 800 nm at 1 kHz repetition rate was used to drive our THz spectrometer. About ~1 mJ pulse energy is used to generate the THz radiation in the air-plasma, while 40 μJ pulse energy is employed for THz detection by air-biased coherent detection (ABCD).

The generation laser beam is focused by a lens and at the position between the lens and the beam focus a frequency-doubling β-BBO crystal is placed. The fundamental beam and its second harmonic (SH) generated in the β-BBO crystal thus co-propagate and create a plasma filament along the focal region. The ionization of air in this two-color laser field leads to the generation of the THz signals with essentially the same bandwidth as that of the initial ultra-short laser pulse [14,18–20]. Similarly, the detection of these ultra-short THz transients occurs via THz field-induced 2nd-order optical nonlinearity of air. As briefly explained below, ABCD can be considered as a refinement of THz field-induced second harmonic generation (T-FISH) [13,14,21]. It is important to note that, unlike in the THz generation mechanism, in the detection process the air is not ionized by the laser or THz fields. Our spectrometer, shown in Fig. 1, employs a commercially-available ABCD detector (ZAP® by Zomega) for the THz pulse sampling. In the detector the optical gating beam and the THz beam are both focused at the same spot between two electrodes (Fig. 1).

#208438 - $15.00 USD Received 17 Mar 2014; revised 9 May 2014; accepted 9 May 2014; published 15 May 2014

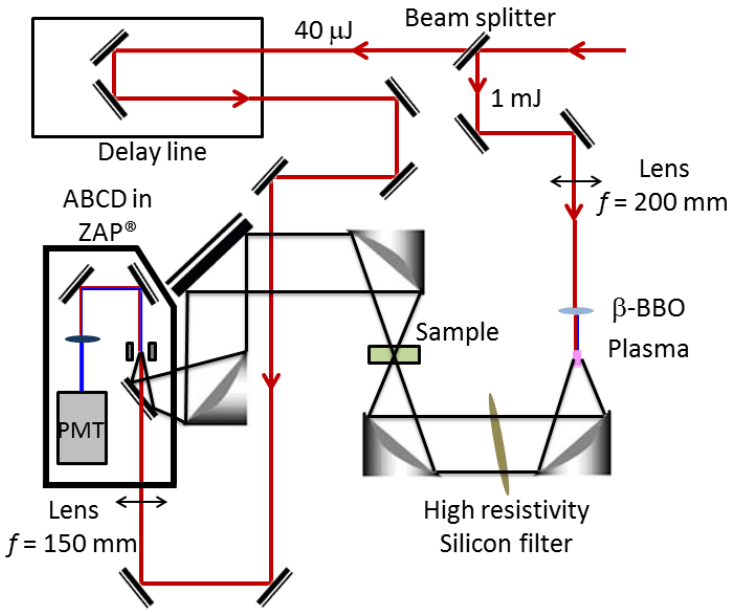

Fig. 1. Ultra-broadband THz TDS setup based on THz plasma generation via two-color laser mixing in air and ABCD detection.

The voltage between the electrodes is switched at 500 Hz, corresponding to half of the laser repetition rate, between the levels of ± 1.5 kV. The presence of the external electric bias E_{bias} in combination with the THz field E_{THz} induces 2nd-order nonlinearity in the air, leading to the generation of the second harmonic of the gating laser pulse. The intensity of the SH is proportional to $(E_{bias} + E_{THz})^2$. The cross term in this square is proportional to the THz field, and can be isolated by means of lock-in techniques. As a result, the electric field of the THz pulse, including its phase, is sampled as a function of the delay between the THz and gating laser pulses [13]. In the experiment, the SH light passing through the electrodes is filtered from the residual fundamental component and detected by a photomultiplier tube (PMT), as shown in Fig. 1. The PMT current as a function of the time delay between the optical gate and the THz pulses is thus the observable of the ABCD measurement. We note here, that the air-plasma filament produces a conically-shaped THz beam [22], which however can be described as a Bessel-Gauss beam with a bell-shaped profile at its waist when focused [23]. Therefore, the experimental geometry typical for a standard THz TDS system [4] is possible with THz air-photonics sources and detectors.

Figure 2(a) provides an example of the measured time-domain data: the black curve is the reference pulse and the red curve is the sample pulse, i.e. the pulse after transmission through the sample, a 0.47 mm thick film of PA6. The reference, incident THz pulse, has the duration of less than 50 fs, and its spectrum extends to the frequencies of about 20 THz, closely matching the duration and the bandwidth of the laser pulse used for the THz generation. The transmitted, sample THz pulse is delayed, reduced in amplitude, and substantially reshaped with respect to the reference due to dispersion, reflection and absorption experienced in the sample. Resonant absorption lines, related to different polar vibrational modes of PA6, clearly appear in the amplitude spectra calculated by discrete Fourier transformation of the time domain signals (Fig. 2(b)). All our measurements were performed at room temperature, and the THz beam path was purged with dry nitrogen to eliminate the THz absorption by water vapor. In frequency domain the amplitude transmission function T at THz frequencies f, through a sample of thickness d and refractive index $\tilde{n} = n + i\kappa$ can be written as follows [24]:

#208438 - $15.00 USD Received 17 Mar 2014; revised 9 May 2014; accepted 9 May 2014; published 15 May 2014

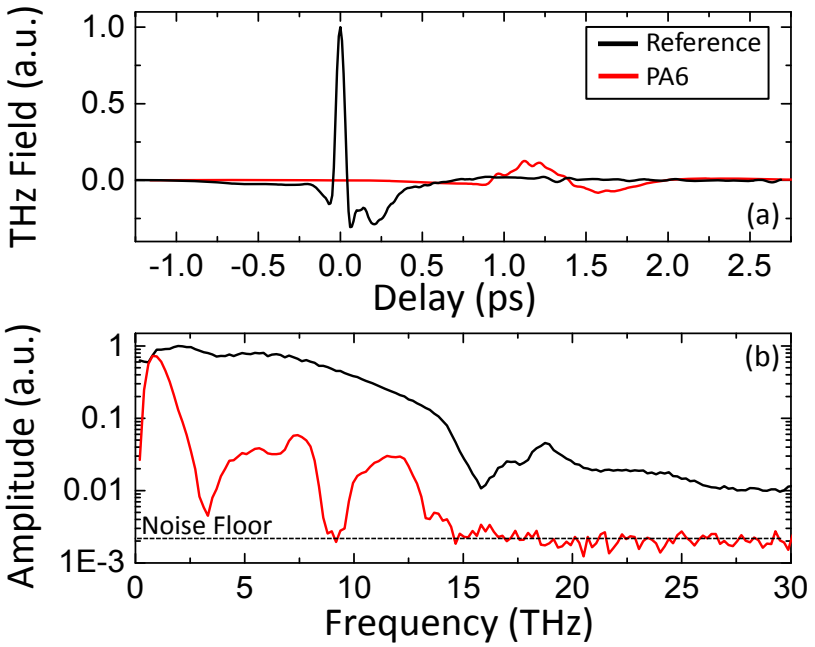

Fig. 2. (a) THz pulses generated and detected in our THz air photonics spectrometer in case of free propagation in air (black) and when transmitted through a 0.47 mm thick sample of PA6 (red). The pulses were normalized to the maximum field of the reference. (b) The corresponding amplitude spectra, obtained from discrete Fourier transforms of the time domain traces.

$$T(\Omega)=\frac{E_s(f)}{E_r(f)}=\frac{4n_{air}\tilde{n}}{(n_{air}+\tilde{n})^2}\cdot\exp\left[-i(\tilde{n}-n_{air})\frac{2\pi fd}{c}\right]\cdot FP(f), \qquad (1a)$$

where E_r and E_s are respectively the reference and sample THz field, n_{air} is the refractive index at THz frequencies of dry air ($n_{air}=1$) and FP is the Fabry-Perot term, which accounts for multiple internal reflections of the THz pulse within the sample, namely:

$$FP(f)=\sum_{m=0}^{N-1}\left\{\left(\frac{\tilde{n}-n_{air}}{\tilde{n}+n_{air}}\right)^2\cdot exp\left[-2i\tilde{n}\frac{2\pi fd}{c}\right]\right\}^m. \qquad (1b)$$

The sum in Eq. (1b) runs over the number of the total transmitted pulses (N) recorded in the time window of the experiment.

The inclusion of multiple reflections in the data processing increases the accuracy of data analysis especially in the case of very thin films [24]. For example, the main transmitted THz pulse through the PTFE sample (30 μm thick) was the result of interference of multiple internal echoes. In the case of thick and highly transparent samples like LDPE and TOPAS® (respectively 0.51 mm and 0.25 mm-thick) the multiple internal reflections were clearly distinguishable in the time-domain data (not shown). The time delay between the main pulse and the first echo was 5.18 ps and 2.54 ps for LDPE and TOPAS® samples, respectively. The chosen scanning time window was selected so that the etalon was not included (4 ps and 4.5 ps long scans for LDPE and TOPAS®, respectively). For the 0.47 mm thick sample of PA6 (Fig. 2), only the transmission of the main pulse was detectable above the noise level since this material was highly absorbing. The frequency resolution of our measurements is given roughly by the inverse of the time window (~250 GHz). Using Eqs. (1a) and (1b) for each sample we derived the real and the imaginary refractive index spectra, respectively $n(f)$ and $\kappa(f)=\alpha(f)c/4\pi f$, where $\alpha(f)$ is the power absorption coefficient of the material, and

#208438 - $15.00 USD Received 17 Mar 2014; revised 9 May 2014; accepted 9 May 2014; published 15 May 2014

the dielectric function $\tilde{\varepsilon}(f)=\tilde{n}(f)^2$. The measurements were repeated several times for each sample in order to reduce the statistical noise. From the individual sets of spectra we could estimate the error in the complex refractive index (data shown in the next Section) as the standard deviation of each set of measurements.

As described in [25], depending on the signal-to-noise ratio of the measurement, the frequency-dependent maximal measurable absorption coefficient $\alpha_{max}(f)$ can be calculated. This quantity marks the limit of reliability in the determination of the optical constants of the material of interest, with the reliability criterion being $\alpha(f)<\alpha_{max}(f)$. In the measured spectra shown in the next Section, the spectral areas not satisfying the above criterion will be marked with grey bars.

2.2 Results and discussion

In this Section we demonstrate our experimental results. The first part is dedicated to such materials as LDPE and TOPAS®, which were found to have negligible dispersion of refractive index and negligible absorption all across the frequency range 2-15 THz, making them technologically relevant for ultra-broadband THz photonics applications. Feature-rich spectra of materials like PA6 and PTFE are discussed in the second subsection. By referring to previous studies, we identified the most prominent spectral features and, where possible, we assigned them to their microscopic origin. We note here that the physical properties of these polymeric compounds may vary significantly depending on the exact manufacturing and specifications. Nevertheless, as shown in this Section the results of our spectroscopy are in general agreement with previous measurements using FTIR spectroscopy or conventional low-bandwidth THz TDS.

A summary of our measurements is given in Table 1. Here we report the refractive index variation range, the central frequencies of resonant modes, the measured absorption coefficient at the resonant frequency, and their molecular assignment according to the literature. At the end of Section 2.2.2 it will be shown that the ultra-broadband THz dielectric functions of PTFE and PA6 can be successfully reproduced using the multiple-Lorentzian model. This may provide a more quantitative insight on the microscopic mechanisms underlying the THz dielectric properties of such compounds.

Table 1. 2-15 THz Refractive Index Variation Range, Absorption Coefficients at the Resonant Frequencies f_0, and their Molecular Assignment for Different Polymeric Compounds.

Polymer	n_{min}	n_{max}	$f_0 @ \alpha$ [THz]	$\alpha(f_0)$ [cm^{-1}]	Molecular origin	Reference
LDPE	1.523	1.526	2.1	1.6 ± 0.8	LM	[5,26,27]
			2.8	2.1 ± 0.7	LM	
			16.3*	–	–	
TOPAS®	1.522	1.525	15*	–	–	[5,17]
PTFE	1.312	1.755	1.5*	–	LM	[28–31]
			6.1	$(5 \pm 1.5)\cdot 10^2$	CF_2 twisting	
			15.5*	–	CF_2 (rocking/wagging)	
			16.5*	–	CF_2 (rocking/wagging)	
PA6	1.587	1.817	3.1-3.4	$(2.2 \pm 0.2)\cdot 10^2$	HB	[32–35]
			6.6	$(1.31 \pm 0.04)\cdot 10^2$	SV	
			8.82*	–	SV	
			9.51*	–	SV	
			13.4	$(2.2 \pm 0.3)\cdot 10^2$	SV	
			15.69*	–	SV	
			17.37*	–	SV	

(*) Literature values for resonant frequencies located outside the reliable spectral window.
LM: Lattice Mode; HB: Hydrogen Bond; SV: Skeletal Vibration.

#208438 - $15.00 USD Received 17 Mar 2014; revised 9 May 2014; accepted 9 May 2014; published 15 May 2014

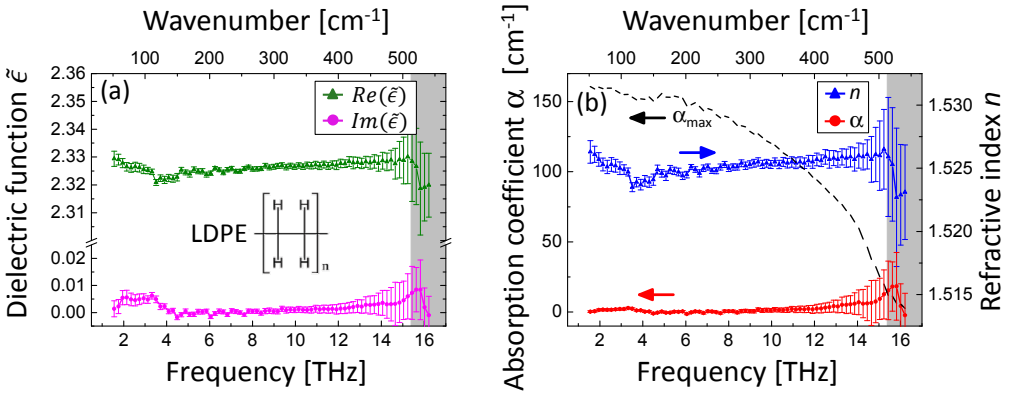

Fig. 3. LDPE: (a) Real (green) and imaginary (magenta) part of the dielectric function. (b) Absorption coefficient (red-left ordinate axis) and refractive index (blue-right ordinate axis). Dashed black line is the maximum absorption that can be reliably measured by our spectrometer (left ordinate axis).

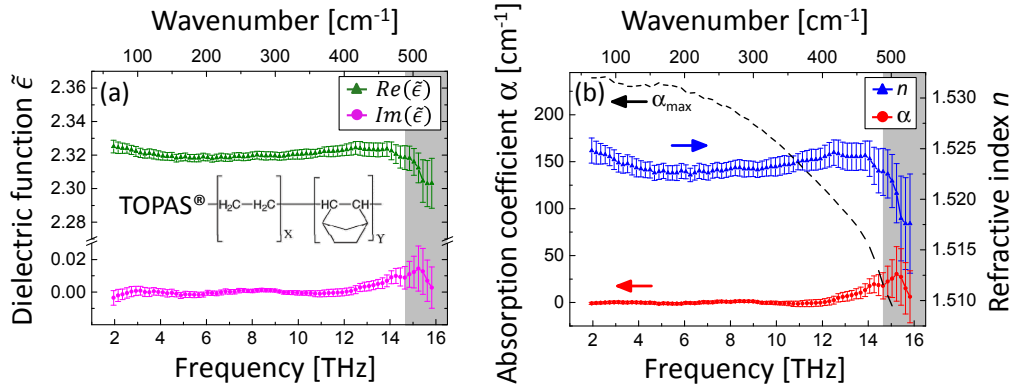

Fig. 4. TOPAS®: (a) Real (green) and imaginary (magenta) part of the dielectric function. (b) Absorption coefficient (red-left ordinate axis) and refractive index (blue-right ordinate axis). Dashed black line is the maximum absorption that can be reliably measured by our spectrometer (left ordinate axis).

2.2.1 LDPE and TOPAS®

Low-density polyethylene is a non-polar olefin polymer commonly found in everyday life as plastic wraps. The structure of polyethylene (PE) is formed by both crystalline and amorphous domains of CH_2 chains. The grade of crystallinity and the percentage of branching mark the substantial distinction between the two most common types of PE: high and low density PE, respectively HDPE and LDPE. Our sample of LDPE is a semi-transparent film prepared by compression molding from pellets of PE distributed by Micro Powders Inc.

In Fig. 3 the measured refractive index, the absorption spectra and complex-valued dielectric function of LDPE are shown. The refractive index is largely constant across the whole spectral range, with an average value of 1.524 ± 0.002. The absorption was found to be negligibly small across the entire spectroscopy window. The slow rise of the index and absorption spectra at higher THz frequencies can be attributed to the tail of the 16.3 THz band reported in [26]. At low frequencies the only exceptions to this featureless behavior are represented by the very weak and broad bands centered at 2.1 THz and 2.8 THz, reported previously and attributed to translational lattice modes, respectively along the *b* and *a* axis of the unit cell [5,27]. The faint and broad features shown by LDPE are good indicators of a low crystallinity grade as well as lattice disorder and pronounced branching.

#208438 - $15.00 USD Received 17 Mar 2014; revised 9 May 2014; accepted 9 May 2014; published 15 May 2014

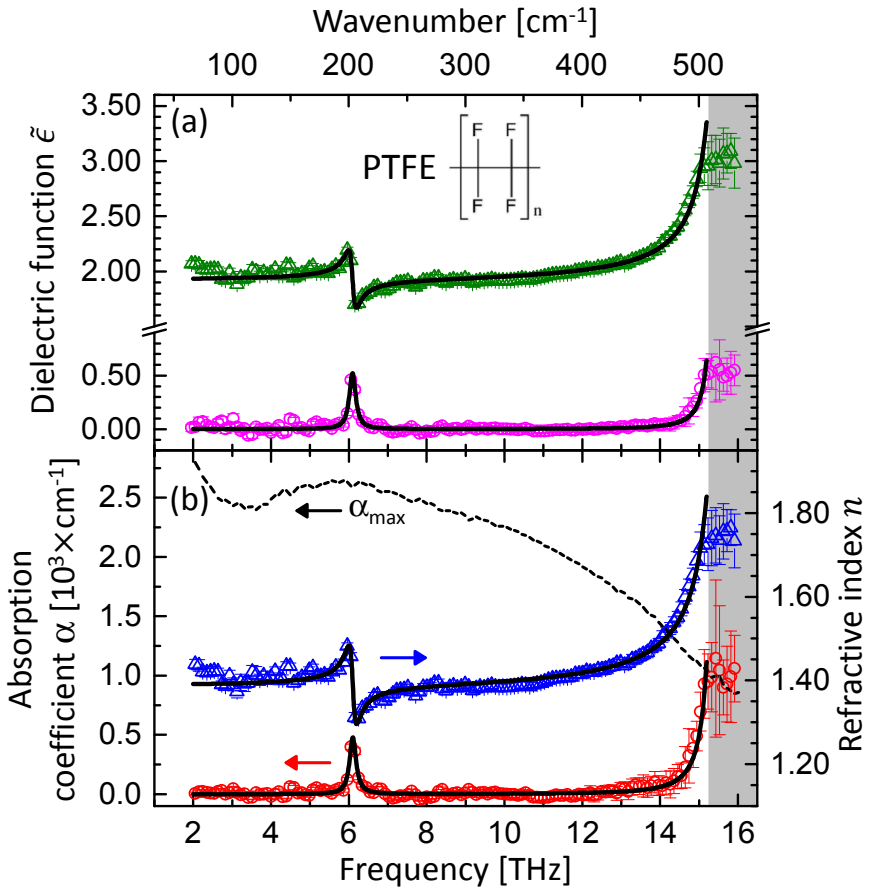

Fig. 5. PTFE (Teflon®): (a) Real (green) and imaginary (magenta) part of the dielectric function. Black lines are fits based on two Lorentzian resonant modes. (b) Absorption coefficient (red-left ordinate axis) and refractive index (blue-right ordinate axis). Black lines are the re-calculated index and absorption coefficient. Dashed black line is the maximum absorption that can be reliably measured by our spectrometer (left ordinate axis).

Our TOPAS® sample (cyclic olefin/ethylene copolymer) was a thin transparent film commercialized by Topas Advanced Polymers. The measured ultra-broadband THz spectra of TOPAS® are shown in Fig. 4. Low dispersion and negligible absorption are again the dominant features in the entire frequency range up to about 14 THz. The average index 1.523 ± 0.002 is also very similar to that of LDPE. The absorption coefficient and the refractive index somewhat increase at higher frequencies (>12 THz), likely due to the presence of an absorption band centered around 15 THz as mentioned in [17]. As in the case of LDPE, low index dispersion and absorption in TOPAS® are mostly due to a weak crystalline structure and to the absence of polar bonds in the polymer chain [5]. The properties shown by LDPE and TOPAS® are particularly attractive for ultra-broadband THz photonic applications. These compounds are usually employed for optical components (e.g. lenses and windows) for low THz frequencies < 4 THz; our studies demonstrate that the same materials, and hence *exact same optical components*, can be used at frequencies up to 14-15 THz just as successfully.

2.2.2 PTFE and PA6

In contrast to the above materials, polytetrafluoroethylene (PTFE, also kwon as Teflon®) and especially polyamde-6 (PA6) show significant dispersion and absorption features in the range 2-15 THz (Figs. 5 and 6). A commercially-available sheet of PTFE was used as a sample.

#208438 - $15.00 USD Received 17 Mar 2014; revised 9 May 2014; accepted 9 May 2014; published 15 May 2014

PTFE consists of the chains of CF_2 forming amorphous and partially ordered crystalline domains which are called spherulites, because of their spherical shape. Despite of the apparent simplicity of the CF_2 chain which may seem similar to that of PE, the presence of polar bonds along the backbone chain and its helical structure make the physical properties of this material very different from those of PE. The spectral assignment and the crystalline structure of PTFE (existing in at least three different phases in the temperature range 273-313 K at ambient pressure) has been discussed extensively [28–30,36].

Points in Fig. 5 show the measured THz spectra of PTFE in the 2-15 THz range. The isolated feature at a frequency of 6.1 THz is assigned to the CF_2 twisting mode [28,30]. At low frequencies (2-4 THz), a spectrally flat refractive index and negligible absorption losses are found. The weak and broad 1.5 THz band (which is below the frequency range of our experiment) originates from different lattice modes distinguishable only at low temperatures, and here apparent from the small anomalous index dispersion at 2-3 THz [28]. A similar low-dispersive behavior is also registered in the range 7-13 THz. In this region several weak absorption features were previously reported in the literature [7,28,31], which are however not clearly distinguishable in our measurements. At the highest frequencies of our spectral range above 14 THz, the onset of a strong absorption peak is observed. This is consistent with the results of infrared spectroscopy, from which bands located at 15.5 THz and 16.5 THz were found. The assignment of these bands is not completely uniform in the literature: CF_2 rocking or wagging modes are both supported by theoretical calculations [28,30].

The last material described in this paper is PA6, also known as Nylon 6. This polymer is commonly used in the production of goods requiring high resistance like ropes, clothes or strings for musical instruments. A complex dispersive index behavior and several pronounced absorption features are clearly visible in the 2-15 THz range for this material, as shown in Fig. 6. The strong absorption peak centered around 3.2 THz has been reported previously and attributed to the translational motion of amide groups in the direction of inter-chain hydrogen bonds [32]. As shown in Fig. 6(b), the 8.6-9.6 THz region is characterized by a very strong absorption reaching values > α_{max}, which is beyond the reliability limits of our measurements. In principle, the number of absorption bands (one or perhaps more) at these frequencies cannot be inferred reliably taking into account only the absorption spectrum in this spectral vicinity. However, the rather abrupt change in the slope of the refractive index found in this spectral range suggests the presence of two resonant modes, in good agreement with the reports of FTIR measurements for this frequency range [34,35]. These two peaks centered at 8.82 THz and 9.51 THz are fingerprints of the two different structures of PA6: respectively the α-PA6 with the CONH group coplanar to the methylene group planes and the γ-PA6 which has the CONH group perpendicular to those planes. Usually both forms are present in different degrees of disorder, as reported in [33,34]. The presence of the α-form in our PA6 sample is substantiated by the pronounced shoulder at 6.63 THz [33,34] previously attributed to a torsional vibration mode of the methylene chain [35]. At even higher frequencies one can identify the band centered at 13.4 THz (Fig. 6(b)). The latter has been reported and identified in the literature as the bending of the CH_2 chain coupled with the in-plane bending of the C = O group [35]. Further infrared-active vibrational modes are expected beyond our frequency window, such as the bands centered around 15.69 THz and 17.37 THz [35]. The presence of these bands is likely the reason of the index rise found at frequencies above 14 THz.

The measured dielectric function of PTFE and PA6 in the 2-15 THz range can be well reproduced by the Lorentz oscillator model [37], as shown by the black lines in Figs. 5 and 6. In this model the complex-valued dielectric function of a material affected by N infrared-active vibrational modes can be described by the following equation:

$$\tilde{\epsilon} = \epsilon_\infty + \sum_{j=1}^{N} \frac{\Omega_j^2}{\left(\omega_{0j}^2 - \omega^2\right) - i\gamma_j\omega}, \tag{2}$$

#208438 - $15.00 USD Received 17 Mar 2014; revised 9 May 2014; accepted 9 May 2014; published 15 May 2014

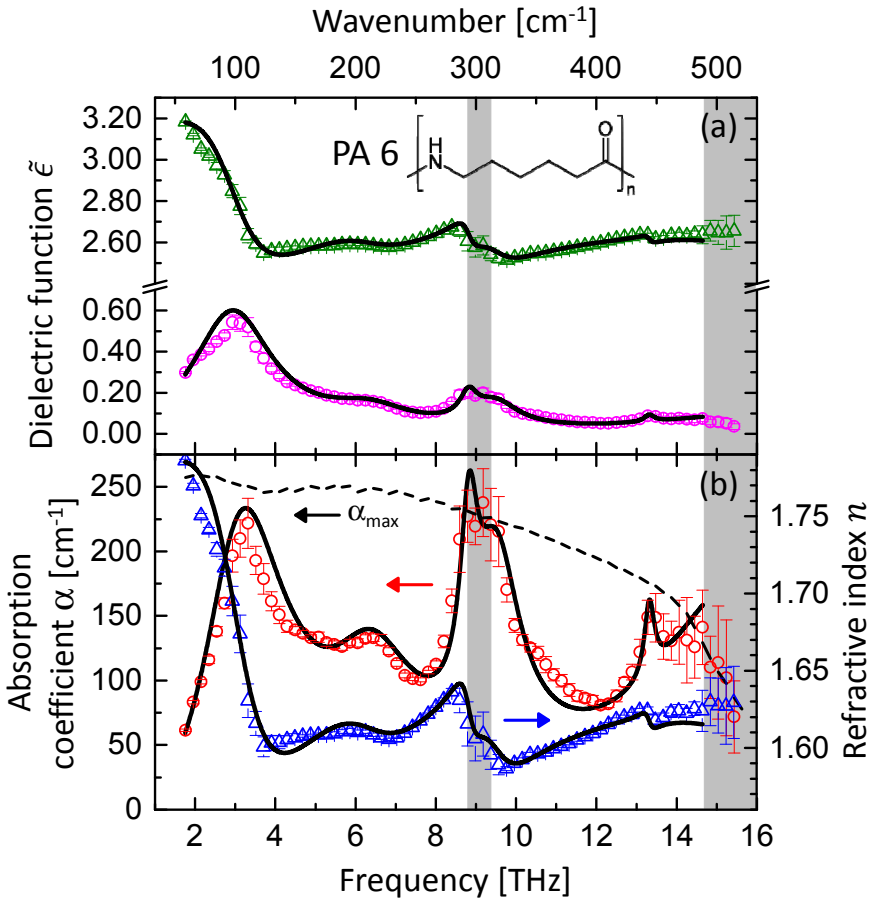

Fig. 6. PA6: (a) Real (green) and imaginary (magenta) part of the dielectric function. Black lines are fits based on six Lorentzian modes. (b) Absorption coefficient (red-left ordinate axis) and refractive index (blue-right ordinate axis). Black solid lines are the re-calculated index and absorption coefficient. Dashed black line is the maximum absorption that can be reliably measured by our spectrometer (left ordinate axis).

where ϵ_∞ is the permittivity constant in the high frequency limit and, Ω_j, $f_{0j} = \omega_{0j} / 2\pi$ and γ_j are respectively the oscillator strength, the resonance THz frequency and the damping constant of the *j*-th resonant mode. The dielectric function of PTFE was fit by using two resonances, while six resonances describe the dielectric function of PA6 (black solid lines in Figs. 5(a) and 6(a)). The agreement between this simple model and the experimental data is excellent proving that the 2-15 THz response of these materials is dominated by resonant processes. The fit parameters for the dielectric functions of PTFE and PA6 are summarized in Tab. 2. For the highest-frequency modes with the resonance frequencies outside of our spectroscopy window 2-15 THz, the mode parameters were estimated from the observed shoulders of these spectral lines (15.5 THz mode in the case of PTFE, and 15.69 THz mode for PA6, respectively). In Figs. 5(b) and 6(b) the refractive index and absorption spectra for PTFE and PA6 are shown along with the fits corresponding to the above dielectric functions.

As a final remark, we note that the strong far-infrared absorption modes both for PTFE and PA6 will probably prevent their ultra-broadband THz photonics applications. However, the use of PTFE for applications in the narrower spectral bands below 4 THz and in the 9-11

#208438 - $15.00 USD Received 17 Mar 2014; revised 9 May 2014; accepted 9 May 2014; published 15 May 2014

THz range is still possible, given their spectrally-flat refractive index and negligible absorption at these frequencies.

Table 2. Lorentzian Fit Parameters for the Dielectric Functions of PTFE and PA6.

Polymer	ϵ_∞	$\omega_{0j}/2\pi$ [THz]	$\Omega_j/2\pi$ [THz]	γ_j [THz]
PTFE	1.84	6.1	0.6	0.2
		15.5*	16.7	0.3
PA6	2.63	3.2	4.4	2.5
		6.45	1.6	2.5
		8.82*	0.5	0.5
		9.51*	1.6	1.4
		13.3	0.1	0.3
		15.69*	6.8	5.3

(*) Constrained parameters applied to the bands outside the reliable spectral window.

3. Conclusions

In this work we have presented the results of ultra-broadband THz spectroscopy of several common polymers in the frequency range 2-15 THz, to the best of our knowledge for the first time. For these measurements a THz TDS spectrometer solely based on THz air-photonics for both generation and detection of sub-50 fs THz transients was used. In this fashion, we have characterized the refractive index and absorption spectra of low-density polyethylene (LDPE), cyclic olefin/ethylene copolymer (TOPAS®), polyamide-6 (PA6), and polytetrafluoroethylene (PTFE).

In contrast to previous studies performed using FTIR [26–29,31–35], THz TDS provides a unique access to both the real and the imaginary part of the dielectric function. Besides, unlike FTIR, THz TDS is an ultrafast technique which can be easily used in pump-probe arrangement, thus directly yielding the dynamics of the ultra-broadband THz response of material of interest under ultrafast illumination. In case of an air-photonics-based system such as demonstrated here, the time resolution in such measurements can reach sub-50 fs. In our work it was found that LDPE and TOPAS® have spectrally-flat refractive index and negligible absorption in the range 2-15 THz, making them highly suitable for ultra-broadband THz photonics. In particular, this means that such components as windows and lenses originally manufactured for the traditional low-THz range <4 THz can be also successfully used at the frequencies reaching 15 THz. PA6 and PTFE were found to have several resonant absorption modes in the range 2-15 THz, which were assigned, where possible, to their specific molecular origin. A multiple-Lorentzian model was successfully applied to describe the measured dielectric function of PTFE and PA6 in the whole ultra-broadband THz range 2-15 THz, providing valuable quantitative input for the fundamental polymer science.

Our studies confirm the very high potential of air-photonics-based THz TDS as a powerful analytic tool in materials science, allowing the spectroscopy in the range where neither conventional low-THz range THz TDS (efficient below ca. 4 THz), nor the Fourier-transform infrared spectroscopy can provide an adequate performance.

Acknowledgments

We are grateful to Ralf Gente and Martin Koch for providing the samples, to Matthias C. Hoffmann for his advice on building the experiment, and to Ivan Ivanov, Zuanming Jin, Søren Jensen and Davide Donadio for helpful discussions and assistance in data processing. We also thank the Danish Council for Independent Research-Technology and Production Sciences (FTP project ALFIE), EU Career Integration Grant 334324 LIGHTER, and Max Planck Society for financial support.